Publisher: GSA
Journal: GEOL: Geology
Article ID: G33723

Ductile strain rate measurements document long-term strain localization in the continental crust

Emmanuelle Boutonnet[1,2], Philippe Hervé Leloup[1], Caroline Sassier[3], Véronique Gardien[1], and Yanick Ricard[1]

[1]*Laboratoire de Géologie de Lyon, Université de Lyon, Université Lyon 1, ENS-Lyon, CNRS, 2 rue Raphaël Dubois, 69622 Villeurbanne, France*

[2]*Institute of Geosciences, Johannes Gutenberg University Mainz, J.-J.-Becher-Weg 21 D-55128 Mainz, Germany*

[3]*Department of Geosciences, University of Oslo, boks 1047, Blindern, 0316 Oslo, Norway*

ABSTRACT

Quantification of strain localization in the continental lithosphere is hindered by the lack of reliable deformation rate measurements in the deep crust. Quartz-strain-rate-metry (QSR) is a convenient tool for performing such measurements once calibrated. We achieve this calibration by identifying the best piezometer-rheological law pairs that yield a strain rate in agreement with that measured on the same outcrop by a more direct method taken as a reference. When applied to two major continental strike-slip shear zones, the Ailao Shan-Red River (ASRR) and the Karakorum, the calibrated QSR highlights across-strike strain rate variations, from < 1×10^{-15} s^{-1} in zones where strain is weak, to > 1×10^{-13} s^{-1} in zones where it is localized. Strain rates integrated across the shear zones imply fast fault slip rates on the order of 1.1 (Karakorum) and 4 cm yr^{-1} (ASRR) proving strong strain localization in these strike-slip continental shear zones.

INTRODUCTION

The extent to which deformation in the continental crust is strongly localized in narrow zones, as it is in the oceanic lithosphere, remains debated. Whilst some argue that continental deformation during collision is mostly localized along few narrow discontinuities (e.g., Tapponnier et al., 2001), the continental crust and lithosphere are commonly modeled as a viscous media in which deformation is pervasive (e.g., Beaumont et al., 2001). This discussion is fundamental to our knowledge of the continent deformation and evolution, but is hindered by the lack of deformation rate measurements in the deep crust. If rates lower than 10^{-15} s^{-1} or higher than 10^{-13} s^{-1} are used to define "stable" or highly deforming zones (Pfiffner and Ramsay, 1982), they have been effectively measured only in a handful of cases (Christensen et al., 1989; Müller et al., 2000; Sassier et al., 2009). There is therefore a need to validate a method of measuring strain rates that could be easily used in various geological settings.

Because quartz is ubiquitous in the continental crust, the quartz-strain-rate-metry (QSR) method, that yields the strain rate from the size of recrystallized quartz grains knowing the deformation temperature, could provide measurements in many geological contexts. However, the QSR results are not reliable because they vary by five orders of magnitude depending on the piezometer-rheological law pair considered. It is therefore necessary to benchmark the QSR using a geological setting where the strain rate is independently known and the thermodynamic conditions accurately defined. This is why we first calibrate the QSR method to determine the most accurate piezometer-rheological law pair, prior to using this calibration to quantify the strain rate variations in two major strike-slip shear zones.

CALIBRATING THE QSR METHOD

Experimental studies show a close relationship (called piezometer) between the average size D of quartz crystals recrystallized during dislocation creep at medium to high temperature and differential stress σ (Shimizu, 2008; Stipp and Tullis, 2003; Twiss, 1977):

$$\sigma = K\,D^{-p} \qquad (1)$$

where p and K are determined experimentally or theoretically.

The QSR method combines this equation with the ductile rheological law in the same thermodynamic condition, that links the strain rate $\dot{\varepsilon}$, the differential stress σ, the temperature T (Gleason and Tullis, 1995), and in some studies the water fugacity f_{H2O} (Hirth et al., 2001; Rutter and Brodie, 2004):

$$\dot{\varepsilon} = d\varepsilon/dt = A\,\sigma^{n}\,f_{H2O}^{\;m}\,e^{-Q/RT} \qquad (2)$$

where the activation energy Q, the prefactor A, and the exponents n and m are determined experimentally, and R is the ideal gas constant. Combining Equations (1) and (2) yields the strain rate $\dot{\varepsilon}$ from the grain size D when the deformation temperature T is known (e.g., Stipp et al., 2002).

The ~1000 km long Miocene left-lateral Ailao Shan Red River (ASRR) shear zone has been interpreted as a plate-like strike-slip boundary separating Indochina and South China blocks (Fig. 1a) (e.g., Leloup et al., 1995). The shear zone crops out as a ~10 km wide belt of high-grade mylonitic gneiss framed by slightly deformed Mesozoic sediments to the north and schists to the south (Fig. 1b). Within the mylonites the site C1 yielded the exceptional opportunity to measure a strain rate from the deformations and ages of three sets of synkinematic dykes (Sassier et al., 2009). A constant strain rate of $3.5 \pm 0.5 \times 10^{-14}\ s^{-1}$ was recorded between 29.9 and 26.8 Ma as well as between 26.8 and 22.6 Ma. This strain rate serves as a reference to calibrate the QSR method applied on two quartz ribbons (YY33 and YY35) sampled 4 m apart at the same site (see Fig. DR1 in the GSA Data Repository[1] for precise sample location). The two quartz ribbons are parallel to the quartzo-feldspatic mylonitic banding. In these rocks, quartz is weaker than feldspar but stronger than biotite. The absence of clasts or of a load bearing framework suggests that deformation occurred in the deformation regime 2 of Handy (1990) where all minerals participate to the deformation.

Grain sizes and shapes of the quartz crystals constituting the two ribbons were measured on thin sections using techniques allowing mapping the grains (electron backscattered diffraction) and their boundaries (optical microscopy). The two samples deformed by dislocation creep accommodated first by grain boundary migration and, later during cooling, by subgrain rotation. The grains recrystallized in the first regime are characterized by amoeboid shapes; in the second regime by angular shapes with angles close to 120°. Average two-dimensional diameters of 62.3±3.0 μm (YY33) and 58.1±2.4 μm (YY35) were measured for the grains deformed by subgrain rotation (Fig. 2). In the case of the piezometers based on the three-dimensional diameters we apply a stereographic correction increasing the grain sizes by a factor $4/\pi$.

The thermodynamic conditions during the recrystallization by subgrain rotation are obtained by combining several methods (Fig. 3):

1-The quartz crystallographic preferred orientation suggests an activation of the <*a*> basal glide system, with minor contribution from the <*a*> prismatic glide system in both samples. This type of deformation occurs for temperatures between 400 and 500°C (Pennacchioni et al., 2010; Stipp et al., 2002).

2-The TitaniQ thermobarometer (Thomas et al., 2010; Wark and Watson, 2006), for an average Ti-content measured by LA-ICP-MS of 14.3±0.4 ppm in YY33 and 14.6±0.9 ppm for

YY35, and a Ti-activity a_{TiO2} = 0.8±0.2 yields a possible domain of P-T equilibrium conditions. A Ti activity ≥0.6 is appropriate for most rocks containing a Ti rich phase (rutile, illimenite, sphene) (Wark and Watson, 2006) or biotite.

3- For YY35, microthermometry of primary and secondary fluid inclusions hosted by the quartz provides a second (isochoric) constraint (Bodnar, 1993) considering the measured homogenization temperatures of 312 ±29°C and salinities of 6.8 ±1.1wt% NaCl.

For YY35, the thermobarometers intersect at T=425 ±38°C and P=130 ±80 MPa (Fig. 3). YY33 data are compatible with these P-T conditions, that are also compatible with the P-T-time path previously proposed for the central Ailao Shan (Leloup et al., 2001), suggesting that subgrain rotation recrystallization occurred around 23 Ma when our reference strain rate was effective. In this context, recrystallization occurs during a retrograde evolution after high temperature (≥500°C) deformation, in which case the TitaniQ thermobarometer is more easily reset than during prograde metamorphism (Grujic et al., 2011).

Using these grain sizes and P-T conditions, several QSR strain rates are calculated using the four piezometers (sets of K and p paramaters (1)) and six power flow laws (sets of Q, A, n, m parameters (2)) published for quartz, i.e. 24 pairs (Fig. 4). The two samples yield similar paleo-strain rates, but which vary between 2.6 $x10^{-18}$ and 4.5 $x10^{-13}$ s^{-1} depending on the piezometer - flow law pair. Taking the temperature and grain size uncertainties into account as well as those of the piezometers and flow laws, yields relatively large error bars on the final result, the main error source being the uncertainty on the deformation temperature (Fig. 4). Most pairs underestimate the site C1 reference strain rate (3.5±0.5 $x10^{-14}$ s^{-1}). The Stipp and Tullis (2003) experimental piezometer corrected for an experimental bias (Holyoke and Kronenberg, 2010) yields satisfactory results when associated with Paterson and Luan (1990) flow law, while

Shimizu's (2008) theoretical piezometer give accurate results when combined with Hirth et al. (2001) flow law. For applications on natural shear zones we rely on that latter pair because its flow law is constrained both by experimental and natural data.

STRAIN RATE MEASUREMENTS FOR TWO MAJOR SHEAR ZONES

By using the QSR method that we have calibrated, we can address the problem of localization of the deformation on two major shear zones for which fast and slow fault slip rates have both been proposed. For all samples, the average grain sizes were precisely measured. The thermodynamic conditions were constrained by the intersection between TitaniQ thermobarometry and P-T-time paths from previous studies and compared with temperature conditions expected from the crystallographic preferred orientations.

The Ailao Shan Red River Shear Zone

The Miocene slip rate of the ASRR has been suggested to be to be rather fast, between 2.8 and 5.3 cm yr^{-1} using geological markers, plate tectonic reconstructions and cooling histories (e.g., Leloup et al., 2001), or conversely to be slower than 1.4 cm yr^{-1} using different geological markers (e.g., Clift et al., 2008). If deformation was homogeneous in space and time within a 10 km-wide shear zone, this would correspond to shear rates between 8.9 $x10^{-14}$ and 1.7 $x10^{-13}$ s^{-1} or below 4.4 $x10^{-14}$ s^{-1}, respectively. Besides the two samples used to calibrate the QSR method at site C1, six others were taken to estimate the strain rates across the shear zone (Fig. 1b).

When plotted along a cross-section of the shear zone, strain rates show a progressive increase from 2.5 $x10^{-15}$ s^{-1} in the SW to 1.3 $x10^{-12}$ s^{-1} in the NE (Fig. 5a), that can be approximated as a linear increase of $\log(\dot{\varepsilon})$. This suggests a strong deformation localization along the NE border of the shear zone and corresponds to an integrated fault slip rate on the order of 4 cm yr^{-1} across it. Such velocity is in the high range of the slip rates proposed for the ASRR. The differential stresses according to (1) range between ~20 and ~52 MPa.

The Karakorum Shear Zone

The > 800 km long right-lateral Karakorum fault zone bounds Tibet to the west (e.g., Tapponnier et al., 2001) (Fig. 1a). Its Neogene-Quaternary slip rate is disputed, with values deduced from geological and geodetic data ranging from below 0.5, up to 1.1 cm yr^{-1} (e.g., Boutonnet et al., 2012; Chevalier et al., 2005; Wright et al., 2004). In the Tangtse area (India), deformation was absorbed within the two narrow Tangtse (see cover image) and Muglib mylonitic strands (e.g., Boutonnet et al., 2012) (Fig. 5b). Five QSR measurements confirm this impression with values above 1.6 $x10^{-13}$ s^{-1} in the two mylonitic strands, and below 1.0 $x10^{-14}$ s^{-1} elsewhere (Fig. 5b). The large size of recrystallized quartz grains in sample LA42 has been taken to imply a very low deformation rate. However, this large size may also indicate that the grain deformed by grain boundary migration in which case the QSR method that we calibrated for subgrain rotation, could be less adequate. The measured shear rates correspond to an integrated fault slip rate between 0.9 and 1.3 cm yr^{-1} close to, but somewhat higher, than previous estimates. The differential stresses according to (1) within the Karakorum shear zone are similar to those of the ASRR ranging between ~24 and ~64 MPa.

CONCLUSION

We calibrated the QSR method in one outcrop of known strain rate and deformation temperature in which various piezometers-flow laws pairs can be tested. For quartz recrystallization in the subgrain rotation regime, the most accurate results are obtained by combining Shimizu's (2008) piezometer with Hirth et al.'s (2001) power flow law. Whilst the absolute deformation rates must be considered with some caution, their relative variation appears robust. As quartz ribbons are ubiquitous, crustal paleo-deformation rates can now be evaluated with an unprecedented spatial resolution.

In the case of the ASRR and Karakorum shear zones, deformation rates appear to be variable across strike in accordance with the qualitative field observations, with narrow (few km wide) zones with strain rates $\geq 10^{-13}$ s^{-1} where most of the deformation localizes. The strain rates in these kilometer wide zones are more than 500 times higher than in the other parts of the exposed shear zones and more than 1000 times higher than in the shear zone surroundings. This implies that a 1 km wide zone of localized strain can accommodate as much deformation as a 1000 km wide block. For the two studied cases, the shear rates, when integrated across strike, are compatible with the fastest slip rates inferred from geologic and geodetic considerations. More strain rate measurements will be crucial for more thoroughly document the ratio between diffuse and localized deformation, but geodynamic models should account for the strong strain localization that seems to characterizes deformation of the continental lithosphere.

ACKNOWLEDGMENTS

We thank 3F INSU-CNRS for funding. We are grateful to C. Lefebvre, L. Menegon, M. Stipp, M. Montagnat, M. Peternell and A. Agranier for discussions and advices, and to C. Gerbi, W. Muller for their constructive reviews.

REFERENCES CITED

Beaumont, C., Jamieson, R.A., Nguyen, M.H., and Lee, B., 2001, Himalayan tectonics explained by extrusion of a low-viscosity crustal channel coupled to focused surface denudation: Nature, v. 414, p. 738–742, doi:10.1038/414738a.

Bodnar, R.J., 1993, Revised equation and table for determining the freezing point depression of H_2O-NaCl solutions: Geochimica et Cosmochimica Acta, v. 57, p. 683–684, doi:10.1016/0016-7037(93)90378-A.

Boutonnet, E., Leloup, P.H., Arnaud, N., Paquette, J.L., Davis, W.J., and Hattori, K., 2012, Synkinematic magmatism, heterogeneous deformation, and progressive strain localization in a strike-slip shear zone. The case of the right-lateral Karakorum fault: Tectonics, v. 31, TC4012, doi:10.1029/2011TC003049.

Chevalier, M.-L., Ryerson, F.J., Tapponnier, P., Finkel, R.C., Van Der Woerd, J., Haibing, L., and Qing, L., 2005, Slip-rate measurements on the Karakorum fault may imply secular variations in fault motion: Science, v. 307, p. 411–414, doi:10.1126/science.1105466.

Christensen, J.N., Rosenfeld, J.L., and DePaolo, D.J., 1989, Rates of tectonometamorphic processes from rubidium and strontium isotopes in garnet: Science, v. 244, p. 1465–1469.

Clift, P., Lee, G.H., Duc, N.A., Barckhausen, U., Long, H.V., and Zhen, S., 2008, Seismic reflection evidence for a Dangerous Grounds miniplate: No extrusion origin for the South China Sea: Tectonics, v. 27, TC3008, doi:10.1029/2007TC002216.

Gleason, G., and Tullis, J., 1995, A flow law for dislocation creep of quartz aggregates determined with the molten salt cell: Tectonophysics, v. 247, p. 1–23, doi:10.1016/0040-1951(95)00011-B.

Grujic, D., Stipp, M., and Wooden, J.L., 2011, Thermometry of quartz mylonites: Importance of dynamic recrystallization on Ti-in-quartz reequilibration: Geochemistry Geophysics Geosystems, v. 12, Q06012, doi:10.1029/2010GC003368.

Handy, M.R., 1990, The solid-state flow of polymineralic rocks: Journal of Geophysical Research, v. 95, p. 8647–8661, doi:10.1029/JB095iB06p08647.

Hirth, G., Teyssier, C., and Dunlap, W.A., 2001, An evaluation of quartzite flow laws based on comparisons between experimentally and naturally deformed rocks: International Journal of Earth Sciences, v. 90, p. 77–87, doi:10.1007/s005310000152.

Holyoke, C.W., and Kronenberg, A.K., 2010, Accurate differential stress measurement using the molten salt cell and solid salt assemblies in the Griggs apparatus with applications to strength, piezometers and rheology: Tectonophysics, v. 494, p. 17–31, doi:10.1016/j.tecto.2010.08.001.

Leloup, P. H., R. Lacassin, P. Tapponnier, U. Schärer, Zhong Dalai, Liu Xiaohan, Zhang Liangshang, Ji Shaocheng, and Phan Trong Trinh, 1995, The Ailao Shan-Red River shear zone (Yunnan, China), Tertiary transform boundary of Indochina: Tectonophysics, V. 251, p. 2-84,. doi: 10.1016/0040-1951(95)00070-4.

Leloup, P.H., Arnaud, N., Lacassin, R., Kienast, J.R., Harrison, T.M., Trinh, P.T., Replumaz, A., and Tapponnier, P., 2001, New constraints on the structure, thermochronology and timing of the Ailao Shan–Red River shear zone, SE Asia: Journal of Geophysical Research, v. 106, p. 6683–6732, doi:10.1029/2000JB900322.

Luan, F.C., and Paterson, M.S., 1992, Preparation and deformation of synthetic aggregates of quartz: Journal of Geophysical Research, v. 97, p. 301–320, doi:10.1029/91JB01748.

Müller, W., Aerden, D., and Halliday, A.N., 2000, Isotopic dating of strain fringe increments: Duration and rates of deformation in shear zones: Science, v. 288, p. 2195–2198, doi:10.1126/science.288.5474.2195.

Paterson, M.S., and Luan, F.C., 1990, Quartzite rheology under geological conditions, *in* Knipe, R.J., and Rutter, E.H., eds., Deformation Mechanisms, Rheology and Tectonics: Geological Society of London Special Publication 360, p. 299–307.

Pennacchioni, G., Menegon, L., Leiss, B., Nestola, F., and Bromiley, G., 2010, Development of crystallographic preferred orientation and microstructure during plastic deformation of natural coarse-grained quartz veins: Journal of Geophysical Research, v. 115, B12405, doi:10.1029/2010JB007674.

Pfiffner, O., and Ramsay, J.G., 1982, Constraints on geological strain rates: Arguments from finite strain rates of naturally deformed rocks: Journal of Geophysical Research, v. 87, p. 311–321, doi:10.1029/JB087iB01p00311.

Rutter, E.H., and Brodie, K.H., 2004, Experimental intracrystalline plastic flow in hot-pressed synthetic quartzite prepared from Brazilian quartz crystals: Journal of Structural Geology, v. 26, p. 259–270, doi:10.1016/S0191-8141(03)00096-8.

Sassier, C., Leloup, P.H., Rubatto, D., Galland, O., Yue, Y., and Lin, D., 2009, Direct measurement of strain rates in ductile shear zones: A new method based on syntectonic dikes: Journal of Geophysical Research, v. 114, B01406, doi:10.1029/2008JB005597.

Shimizu, I., 2008, Theories and applicability of grain size piezometers, the role of dynamic recrystallization mechanisms: Journal of Structural Geology, v. 30, p. 899–917, doi:10.1016/j.jsg.2008.03.004.

Stipp, M., and Tullis, J., 2003, The recrystallized grain size piezometer for quartz: Geophysical Research Letters, v. 30, 2088, doi:10.1029/2003GL018444.

Stipp, M., Stünitz, H., Heilbronner, R., and Schmid, S.M., 2002, The eastern Tonale fault zone: A ‘natural laboratory’ for crystal plastic deformation of quartz over a temperature range from 250 to 700°C: Journal of Structural Geology, v. 24, p. 1861–1884, doi:10.1016/S0191-8141(02)00035-4.

Stipp, M., Tullis, J., Scherwath, M., and Behrmann, J., 2010, A new perspective on paleopiezometry: Dynamically recrystallized grain size distributions indicate mechanism changes: Geology, v. 38, p. 759–762, doi:10.1130/G31162.1.

Tapponnier, P., Zhiqin, X., Roger, F., Meyer, B., Arnaud, N., Wittlinger, G., and Jingsui, Y., 2001, Oblique stepwise rise and growth of the Tibet plateau: Science, v. 294, p. 1671–1677, doi:10.1126/science.105978.

Thomas, J., Watson, E.B., Spear, F., Shemella, P., Nayak, S., and Lanzirotti, A., 2010, TitaniQ under pressure: The effect of pressure and temperature on the solubility of Ti in quartz: Contributions to Mineralogy and Petrology, v. 160, p. 743–759, doi:10.1007/s00410-010-0505-3.

Twiss, R., 1977, Theory and applicability of a recrystallized grain size paleopiezometer: Pure and Applied Geophysics, v. 115, p. 227–244, doi:10.1007/BF01637105.

Wark, D., and Watson, E., 2006, TitaniQ: A titanium-in-quartz geothermometer: Contributions to Mineralogy and Petrology, v. 152, p. 743–754, doi:10.1007/s00410-006-0132-1.

Wright, T.J., Parsons, B., England, P.C., and Fielding, E.J., 2004, InSAR observations of low slip rates on the major faults of western Tibet: Science, v. 305, p. 236–239, doi:10.1126/science.1096388.

FIGURE CAPTIONS

Figure 1. (a) Ailao Shan-Red River (ASRR) and Karakorum (K) shear zones. (b) Cross-section of the ASRR containing site C1 where the QSR method has been calibrated. Adapted from Leloup et al. (1995). The shear zone is framed by the Ailao shan fault (AF) and the Red River fault (RRF). Other samples for which shear strains are measured (see Fig. 5a) are also located.

Figure 2. Sample YY33 (a) and YY35 (b) quartz microstructures on thin-section microphotographs (top) and grain-size distributions (bottom) (Site C1, Ailao Shan-Red River shear zone). Sum of individual normal distributions (dashed Gaussian curves) yields closest size distribution to measured histogram (gray bars). Recrystallization mechanisms fields: BLG—bulging; SGR—subgrain rotation; GBM—grain boundary migration according to Stipp et al. (2010).

Figure 3. Pressure-temperature (P-T) conditions for the quartz recrystallization event by subgrain rotation at site C1 (Ailao Shan-Red River shear zone). Sample YY33 and YY35 recrystallization conditions (T = 425±38°C, P = 130±80 MPa, black cross) are given by the intersection of the TitaniQ thermo-barometer (labeled TiQ) (data in Table DR2) and YY35 fluid inclusions isochors (labeled F.I.) (data in Table DR3). This P-T field is consistent with the quartz deformation temperature indicated by the crystallographic preferred orientation (labeled CPO, details in Fig. DR4), temperature at which α quartz recrystallizes by subgrain rotation and with the central Ailao Shan P-T-time path from Leloup et al. (2001) (ages in Ma in white). Recrystallization mechanisms as in Fig. 2. Temperatures for glide systems activation from Pennacchioni et al., (2010) and Stipp et al. (2002).

Figure 4. Results of the QSR method on samples YY33 and YY35 at site C1 (Ailao Shan-Red River shear zone). Strain rate measured at site C1 (Sassier et al., 2009) and average shear rates for ASRR are plotted for comparison. See Table DR5 for piezometers parameters: S&T (Stipp and Tullis, 2003) ; S&Tc (Stipp and Tullis, 2003) corrected by Holyoke and Kronenberg, (2010) ; T (Twiss, 1977) ; S (Shimizu, 2008). See Table DR6 for rheological parameters: R&B (Rutter

and Brodie, 2004); L&P (Luan and Paterson, 1992); G&T (Gleason and Tullis, 1995); G&Tc (Gleason and Tullis, 1995) corrected by Holyoke and Kronenberg, (2010); H (Hirth et al., 2001), P&L (Paterson and Luan, 1990). When needed, the water fugacity was assumed equal to the hydrostatic pressure. The black frames indicate the piezometer-low law pairs that yield strain rates in agreement with the reference value. The thin error bars are the total uncertainties, the bold ones are linked to the uncertainty on the deformation temperature (T) only.

Figure 5. Sections across two major shear zones showing the local strain rates measured values with the QSR method (black dots), with respect to the lithology (Sc: schist, M: mylonites, Se: sediments, G: undeformed granite, Me: metamorphic). See Table DR7 for detailed results. Dot-dashed lines: shear rate profiles used for the calculation of the integrated shear rates. (A) Ailao Shan Red River (ASRR) shear zone (see Fig. 1b). Light and dark grey horizontal bands indicate bulk strain rates calculated for a 10 km wide shear zone, respectively inferring fast fault slip rates between 2.8 and 5.3 cm/yr, or slow ones between 0.5 and 1.4. (B) Karakorum shear zone, at the latitude of Tangtse village (India). Light and dark grey horizontal bands indicates bulk strain rates calculated for a 8 km wide shear zone, respectively inferring fast fault slip rates between 0.7 and 1.1 cm/yr, or slow ones between 0.1 and 0.5 cm/yr.

[1]GSA Data Repository item 2013xxx, Figures DR1 and DR4, and Tables DR2–DR3, DR5-DR7, is available online at www.geosociety.org/pubs/ft2013.htm, or on request from editing@geosociety.org or Documents Secretary, GSA, P.O. Box 9140, Boulder, CO 80301, USA.

Figure 1
Click here to download Figure: Fig1.eps.pdf

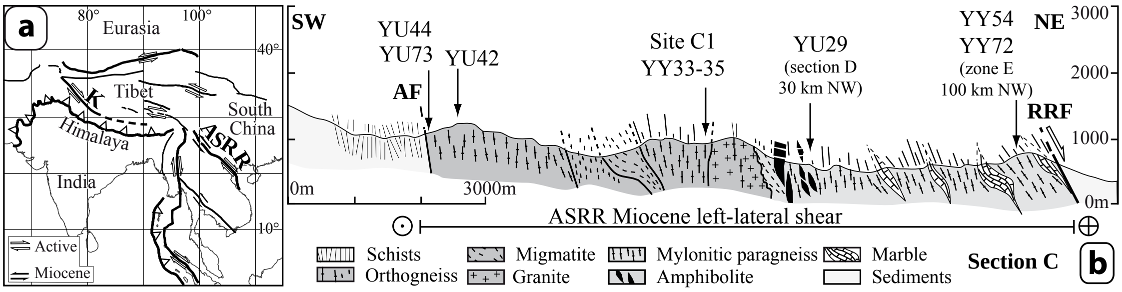

E. Boutonnet - G33723 - Fig. 1 - pdf

Figure 2
Click here to download Figure: Fig2.eps.pdf

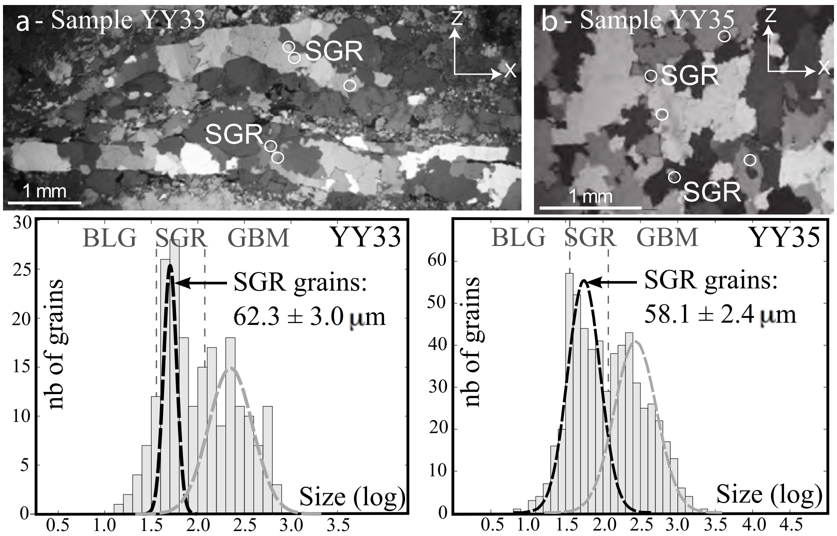

E. Boutonnet - G33723 - Fig. 2 - pdf

Figure 3
Click here to download Figure: Fig3.eps.pdf

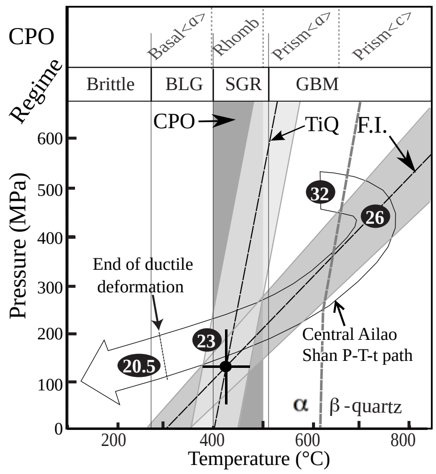

E. Boutonnet - G33723 - Fig. 3 - pdf

Figure 4

Click here to download Figure: Fig4.eps.pdf

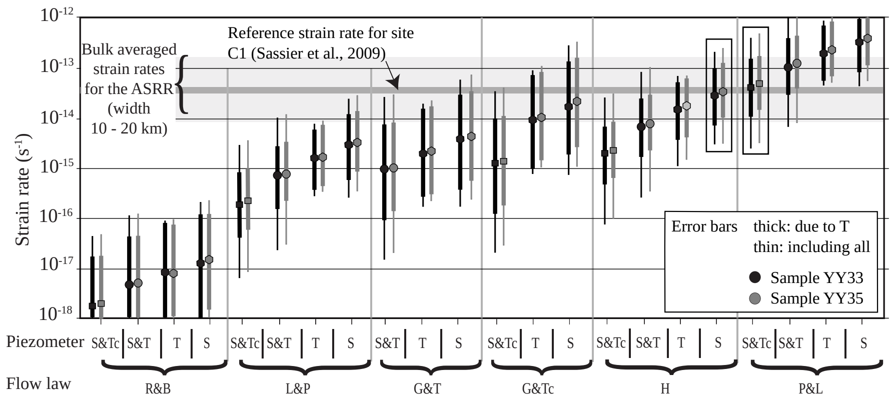

E. Boutonnet - G33723 - Fig. 4 - pdf

Figure 5

Click here to download Figure: Fig5.eps.pdf

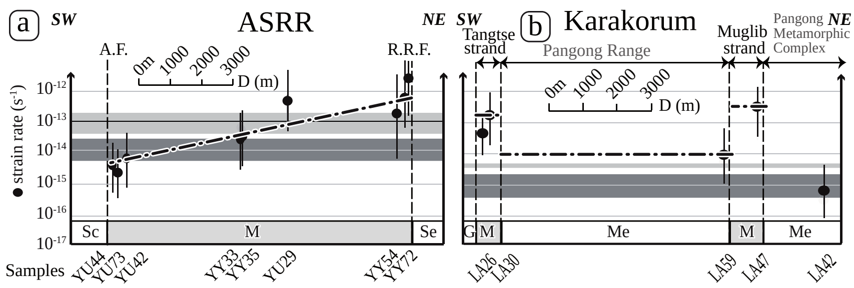

E. Boutonnet - G33723 - Fig. 5 - pdf

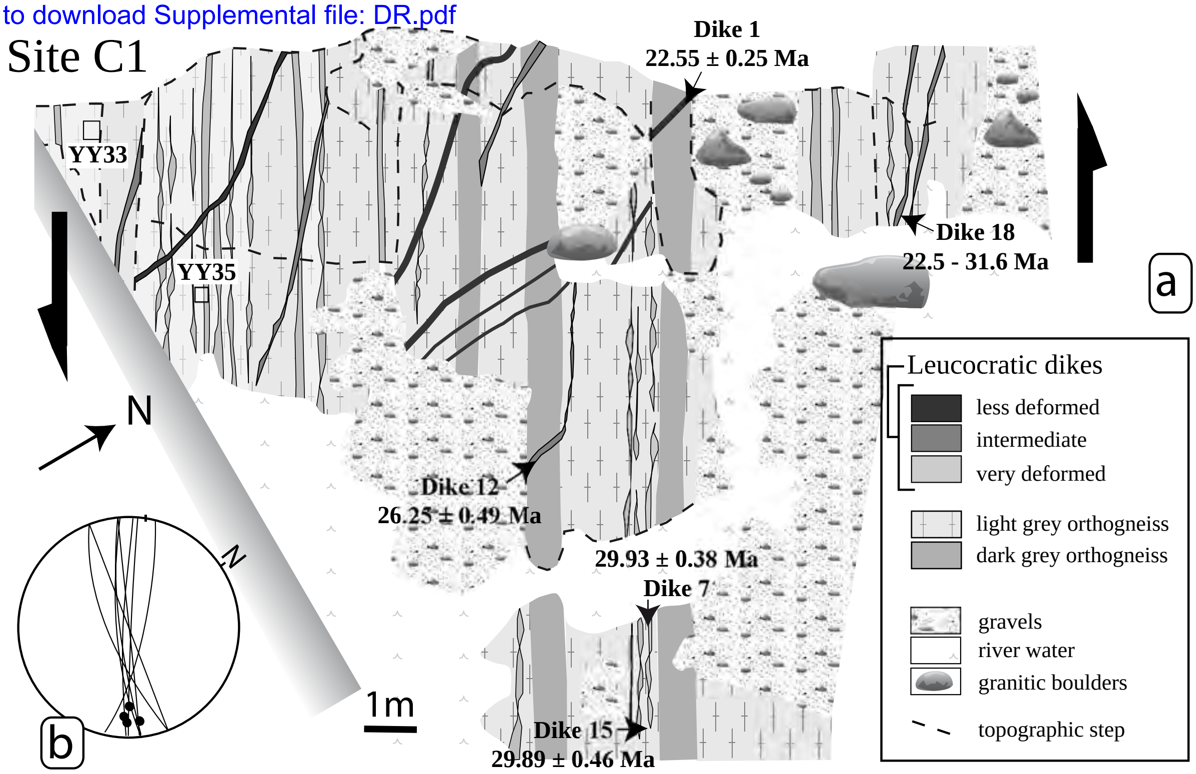

a) Map of site C1modified from Sassier et al. (2009). Samples YY33 and YY35 are located
b) Foliation and lineation geometry at site C1.

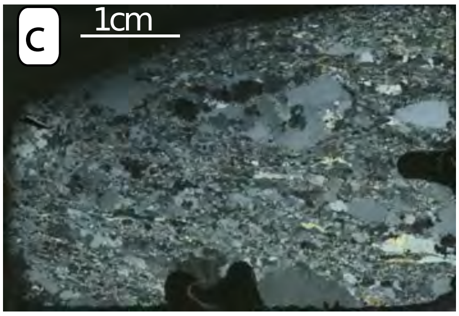

YY33 Thin section (polarized light)

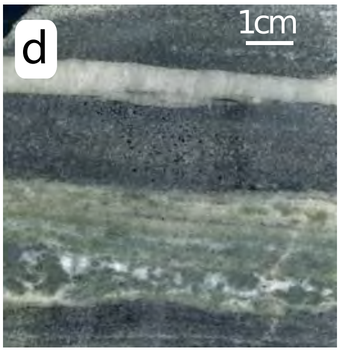

YY35 polished slab showing the quartz ribon where the measurements were performed

Fig. DR1

TABLE DR2. Ti-IN-QUARTZ MEASUREMENTS

Samples characteristics		Analytical characteristics		Average Ti contents (ppm)						
Name	Matrix TiO_2-contents (%) / mineral	Number of points	Accuracy for Ti (% for NIST 612)	Ti from ^{47}Ti (ppm)	err (1σ)	Ti from ^{48}Ti (ppm)	err (1σ)	Ti from ^{49}Ti (ppm)	err (1σ)	Average Ti (ppm)
YY35	0.65 / titanite, oxydes, biotite	10	0,1	**14.8**	0.4	N.A.*	N.A.*	**13.7**	0.5	**14.3 ± 0.4**
YY33	0.65 / titanite, oxydes, biotite	9	0,1	**15.0**	0.7	N.A.*	N.A.*	**14.1**	1.0	**14.6 ± 0.9**
YU29	*N.A. /oxydes, biotite*	10	0,3	**27.4**	2.0	N.A.*	N.A.*	**24.4**	2.1	**25.9 ± 2.1**
YU73	*N.A. /oxydes, biotite*	8	0,2	**4.8**	0.7	**4.0**	0.4	**4.7**	0.5	**4.5 ± 0.5**
YU42	*N.A. /oxydes, biotite*	8	0,2	**10.5**	1.7	**10.2**	2.6	**9.5**	2.1	**10.1 ± 2.1**
YU44	*N.A. /oxydes*	9	0,1	**6.3**	0.5	N.A.*	N.A.*	**5.1**	0.3	**5.7 ± 0.4**
YY54	*N.A. /oxydes, biotite*	7	0,2	**61.9**	1.1	**61.5**	1.3	**61.6**	2.9	**61.7 ± 1.8**
YY72	*N.A. /oxydes, (biotite)*	12	0,2	**40.8**	4.0	**40.8**	3.1	**40.7**	3.8	**40.8 ± 3.6**
LA26	*N.A. /(oxydes)*	13	0,2	**6.4**	0.3	**5.9**	0.4	**6.5**	0.5	**6.3 ± 0.4**
LA30	*N.A. /titanite, (oxydes), biotite*	17	0,2	**5.0**	0.5	**4.3**	0.4	**5.0**	0.6	**4.8 ± 0.5**
LA42	*N.A. /(biotite)*	12	0,2	**1.9**	0.4	**1.4**	0.2	**1.9**	0.3	**1.7 ± 0.3**
LA59	*N.A. /oxydes, biotite*	13	0,2	**4.6**	0.8	**3.6**	0.6	**4.6**	0.8	**4.3 ± 0.7**
LA47	*N.A. /oxydes, biotite*	14	0,2	**4.4**	0.5	**3.9**	0.7	**4.5**	0.3	**4.3 ± 0.5**

*N.A. = not available

Ti concentrations in quartz are determined by ICP-MS (Element XR) coupled to a laser ablation system (Microlas platform and Excimer CompEx Laser, spot diameters of 33 microns and repetition rates of 10 Hz) at the Geosciences Montpellier laboratory (France) and at IUEM Brest (France).

The alignment of the instrument and mass calibration is performed before every analytical session using the NIST 612 reference glass. USGS basalt glass reference materials BCR and BIR are used during experiment as standards.

Masses isotopes are analyzed over 20 cycles for each analysis. ^{27}Al, ^{29}Si, ^{43}Ca and ^{7}Li isotopes are used to monitor the quartz ablation, and ^{85}Rb, ^{86}Sr and ^{137}Ba to control if other mineral inclusions are also ablated.

The internal standard is measured by assuming that the sum of all quartz elements amount to 100%

TABLE DR3. FLUID INCLUSIONS MICROTHERMOMETRY RESULTS - SAMPLE YY35

Fluid inclusions types			Temperatures (°C) **		Isochors: P (bar) = aT(°C) +b ***		Salinity ***	
Fluid inclusion group *	Characteristics	Bubble size (%)	melting	Homogenization	a	b	wt% NaCl	mol/kg
G1	Primary F.I.	18.52	**-4.3**	**311.8**	10.4	-3195.5	6.8	1.2
11 measurements	isolated		1σ: 0.5	1σ: 7.7	± 0.9	± 131.8	± 1.1	± 0.3
G2	Secondary F.I.	12.37	**-4.2**	**311.7**	10.6	-3195.5	6.7	1.2
88 measurements	aligned along trails		1σ: 0.6	1σ: 30.5	± 0.9	± 131.8	± 1.1	± 0.3

* Inclusion groups assemble inclusions with similar geometry, orientation and composition which we interpret as cogenetic

** Measurements are carried out on a Linkam Inc. Heating-Freezing Stage at the LGL-TPE (Lyon). Calibration is performed from synthetic fluid inclusions containing pure water and a CO_2-H_2O mixing. The phase transitions of the fluid inclusions are observed in thick sections (100 um-thick) with an optical microscope between -100°C and +400°C.

*** Isochor equations and salinities are calculated using Zhang and Frantz (1987) and Bodnar (1993)

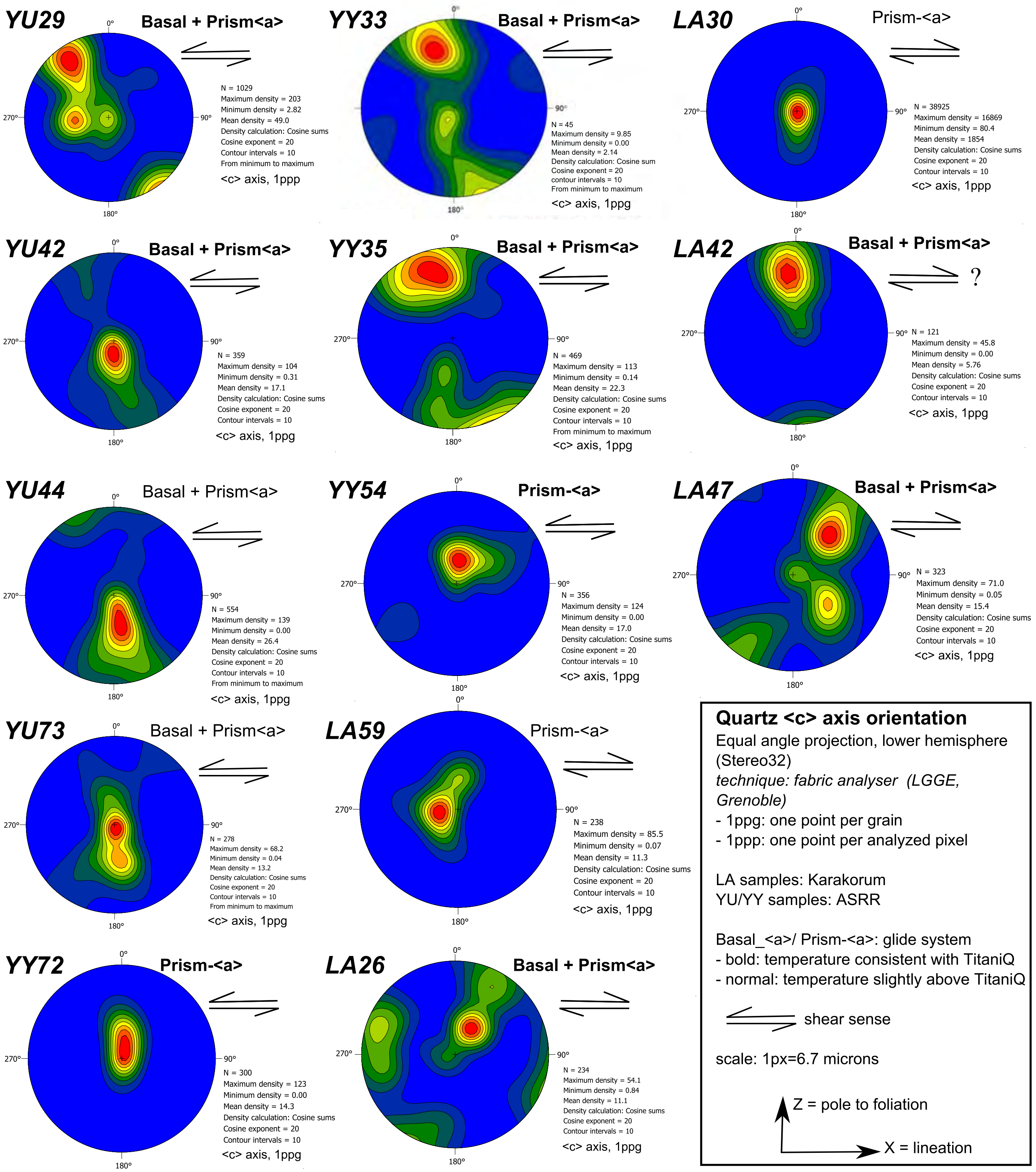

Quartz CPO of samples from the ASRR and Karakorum shear zones.

Figure DR4

Table DR5. Experimentally and theoretically derived parameters for piezometers (equation 1) compiled from the literature.

Piezometer	Calibration type	Recrystallization regime	K (Mpa μm^p)	p
Stipp and Tullis (2003)	Experimental	Bulging	669	0.79
Stipp and Tullis (2003)	Experimental - Corrected by Holyoke and Kronenberg (2010)	Bulging	480	0.79
Twiss (1977)	Theoretical	Subgrain rotation	603	0.68
Shimizu (2008)	Theoretical	Nucleation by Subgrain rotation and Growth by Grain Boundary Migration of α-quartz	217	0.8

Table DR6. Experimentally derived parameters for deformation power flow-laws (equation 2) compiled from the literature.

Flow law	Calibration type	Conditions	Q (kJ mol^{-1})	A (MPa^{-n} s^{-1})	n	m
Luan and Paterson (1992)	Experimental	Dislocation creep	152	4.0×10^{-10}	4	0
Paterson and Luan (1990)	Experimental	Dislocation creep	135	6.5×10^{-8}	3	0
Hirth et al. (2001)	Experimental	Dislocation creep	135	6.3×10^{-12}	4	1
Rutter and Brodie (2004)	Experimental	Dislocation creep	242	1.2×10^{-5}	3	1
Gleason and Tullis (1995)	Experimental	Dislocation creep	223	1.1 x 10-4	4	0
Gleason and Tullis (1995)	Experimental - Corrected by Holyoke and Kronenberg (2010)	Dislocation creep	223	5.1×10^{-4}	4	0

TABLE DR7. QSR-S-H STRAIN RATE MEASUREMENTS IN THE ASRR AND KFZ STRIKE-SLIP SHEAR ZONES

Shear zone/ sample	Lat/Long	Quartz vein size	Recrystalliza - tion regime[a]	Mean grain size measured (microns)	Mean grain size corrected[b] (microns)	Stress[c] (MPa)	Method of Temperature determination	Temperature (°C)	Pressure (MPa)	Hydrostatic pressure (MPa)		Strain rate[d] (s^{-1})
ASRR												
YY33	23.55441° N	mm	SGR	62,3	79.3	36.1	Ti-in-Quartz +	425	130	34		**2.9E-14**
error (1 sigma)	101.91674° E			±1.8	±4.0	±6.7	P-T path	±40	±80	±25	max	2.0E-13
											min	3.1E-15
YY35	23.55441° N	cm	SGR	58,1	74.0	38.1	Ti-in-Quartz +	425	130	34		**3.6E-14**
error (1 sigma)	101.91674° E			±2.4	±3.5	±7.2	microthermometry	±38	±80	±25	max	2.4E-13
											min	4.1E-15
YU44	23.530007° N	cm	SGR	64,4	82.0	41.0	Ti-in-Quartz +	367	110	22		**3.7E-15**
error (1 sigma)	101.910773° E			±2.7	±4.0	±6.7	P-T path	±40	±80	±15	max	2.0E-14
											min	5.5E-16
YU73	23.530007° N	mm	SGR	59,9	76.3	45.4	Ti-in-Quartz +	352	100	18		**2.5E-15**
error (1 sigma)	101.910773° E			±3.0	±4.5	±7.3	P-T path	±40	±80	±13	max	1.3E-14
											min	3.7E-16
YU42	23.530007° N	mm	SGR	79,2	100.9	31.6	Ti-in-Quartz +	402	120	32		**7.0E-15**
error (1 sigma)	101.910773° E			±2.0	±3.0	±5.5	P-T path	±40	±80	±20	max	4.8E-14
											min	7.9E-16
YU29	23.767183° N	mm	SGR	39,8	50.7	46.6	Ti-in-Quartz +	469	150	50		**5.2E-13**
error (1 sigma)	101.710783°E			±1.8	±2.7	±9.7	P-T path	±44	±80	±25	max	4.5E-12
											min	3.4E-14
YY54	24.277583°N	mm	SGR	64,9	82.6	27.2	Ti-in-Quartz +	544	180	79		**6.5E-13**
error (1 sigma)	101.378817°E			±1.8	±2.7	±6.4	P-T path	±51	±80	±32	max	4.8E-12
											min	5.9E-14
YY72	24.43207°N	cm	SGR	32,6	41.5	50.7	Ti-in-Quartz +	507	160	72		**2.7E-12**
error (1 sigma)	101.25493°E			±1.7	±3.0	±11.5	P-T path	±59	±80	±31	max	2.7E-11
											min	1.8E-13
KFZ												
LA26	34.025028°N	cm	SGR	75,6	96.2	35.5	Ti-in-Quartz +	415	350	80		**4.6E-14**
error (1 sigma)	78.171832°E			±1.6	±2.3	±5.7	P-T path	±40	±80	±37	max	2.1E-13
											min	8.7E-15
LA30	34.023361°N	mm	SGR	39,5	50.3	55.4	Ti-in-Quartz +	400	350	80		**1.6E-13**
error (1 sigma)	78.175861°E			±2.3	±3.5	±10.2	P-T path	±40	±80	±37	max	7.6E-13
											min	2.6E-14
LA59	34.052861°N	cm	SGR	91,3	116.3	28.8	Ti-in-Quartz +	393	350	80		**9.2E-15**
error (1 sigma)	78.245889°E			±2.5	±3.7	±4.9	P-T path	±40	±80	±37	max	4.4E-14
											min	1.6E-15
LA47	34.009139°N	mm	SGR	32.0	40.8	66.6	Ti-in-Quartz +	394	350	80		**2.6E-13**
error (1 sigma)	78.303111°E			±1.5	±2.2	±11.7	P-T path	±40	±80	±37	max	1.2E-12
											min	4.6E-14
LA42	33.971194°N	cm	SGR or GBM	134,2	170.9	24.1	Ti-in-Quartz +	347	350	80		**7.3E-16**
error (1 sigma)	78.376750°E			±2.1	±3.1	±3.6	P-T path	±40	±80	±37	max	3.1E-15
											min	1.4E-16

Note: ASRR= Ailao Shan Red River ; KFZ= Karakorum Fault Zone; Recrystallization regime: SGR= sub-grain rotation; BLG= bulging.

Uncertainty calculation takes into account: the experimental measurement errors (LA-ICP-MS, microthermometry, grain size, P-T path, EBSD, Fabric analyser), the errors of equations calibration when available (piezometer, flow law, thermo-barometer) and they are propagated to measure the strain rate.

[a] The recrystallization regime is determined by the shape of the considered grains following criteria of Stipp et al. (2002). [b] Stereographic correction

Stress calculated using: [c]Shimizu (2008) piezometer

Strain rates calculated using: [d]Hirth et al. (2001) power flow law